

TABLE OF CONTENTS

	Page
Acknowledgements	iii
Abstract (English)	v
Abstract (Thai)	vii
List of tables	xii
List of figures	xiii
Abbreviations and symbols	xix
Chapter 1 Introduction	1
1.1 Objectives of this research	11
Chapter 2 Background	13
2.1 General properties of ZnO	13
2.1.1 Crystal structure	13
2.1.2 Electronic band structure	22
2.2 N-type doping of ZnO	24
2.3 Flame spray pyrolysis	26
2.3.1 Particle growth and coagulation	28
2.4 Metal oxide for gas sensor	30
2.4.1 Surface conductive sensors	31
2.4.1.1 Physical and chemical adsorption	32
2.4.1.2 Surface states	35

TABLE OF CONTENTS (Continued)

	Page
2.4.1.3 Sensing mechanism	38
2.4.2 DC resistance transduction	44
2.5 Metal oxide for photocatalyst	45
2.5.1 Mechanism of metal-oxide-assisted photocatalytic degradation	45
2.5.2 Langmuir-Hinshelwood kinetics	53
Chapter 3 Experimental	56
3.1 Materials and instruments	56
3.2 Nanostructure synthesis and characterization	58
3.3 Preparation of sensing films	61
3.4 Gas sensing measurement	62
3.5 Photocatalytic activity testing	63
Chapter 4 Results and discussion	66
4.1 Physical characterization of the synthesized nanostructures	66
4.2 Gas sensing application	73
4.2.1 The effect of operating temperatures on gas response of undoped ZnO and Sn-doped ZnO sensors	75

TABLE OF CONTENTS (Continued)

	Page
4.2.2 The effect of gas species on change in conductivity of undoped ZnO and Sn-doped ZnO sensors	79
4.2.3 The gas response comparison of undoped ZnO and Sn-doped ZnO sensors	84
4.3 Photocatalyst application	88
4.3.1 UV-vis absorption characteristics	88
4.3.2 Phenol and methanol photodegradation properties	93
Chapter 5 Conclusions	99
Appendices	103
Appendix A	104
Appendix B	136
Appendix C	138
References	144
Curriculum Vitae	169

LIST OF TABLES

Table		Page
2.1	Zn-O crystal structure data	14
2.2	Properties of wurtzite ZnO	21
2.3	Primary processes and time estimation on TiO ₂ photocatalytic activity process	47
2.4	Langmuir-Hinshelwood model assumptions	53
3.1	Category of chemicals: Purity, Molecular weight/Density and Company	56
3.2	Instruments used in the experiments	57
4.1	The apparent zero-order rate constants of C ₆ H ₅ OH degradation over Sn-doped samples	96
A.1	Literature reviews of Sn-doped ZnO films	103
A.2	Literature reviews of Sn-doped ZnO particles	116

LIST OF FIGURES

Figure		Page
1.1	Annual number of papers published related to ZnO. Literature search was carried out ISI Web of Knowledge using the keyword “ZnO*” or “Zinc Oxide*”.	3
2.1	Phase diagram for condensed Zn-O system at 0.1 MPa	14
2.2	ZnO crystal structures: (a) cubic rocksalt (B1), (b) cubic zinc blende (B3) and (c) hexagonal wurtzite (B4) (Atoms in grey and black colors refer to Zn and O atoms, respectively.)	15
2.3	Schematic structure of wurtzite ZnO	16
2.4	Labeling of planes in hexagonal symmetry (for sapphire)	18
2.5	Labeling of planes in hexagonal symmetry in the $(tuvw)$ coordinate system	20
2.6	Orientations that are commonly used in wurtzite phase, namely, the $(11\bar{2}0)$ and $(1\bar{1}00)$ planes and associated directions are shown as projections on the (0001) basal plane.	20
2.7	ZnO valence and conduction band structure diagram	24
2.8	Various mechanisms for metal oxide formation by spraying dissolved metal precursors into a high-temperature reaction zone	27

LIST OF FIGURES (Continued)

Figure		Page
2.9	Schematic of titania synthesis by TiCl_4 oxidation by the “chloride” process	30
2.10	Lennard-Jones model for physical and chemical adsorption as a function of the energy of the system, and adsorbate/adsorbent distance: (a) physical adsorption and (b) chemical adsorption	33
2.11	Isobar of typical adsorption: (I) physisorption, (II) irreversible transition and (III) chemisorption	34
2.12	Madelung model of ionic solid MX ; χ is the electron affinity and I is the ionization potential.	36
2.13	Schematic diagram model on band bending of wide bandgap semiconductor metal oxides after ionosorption of oxygen on surface sites. E_C , E_V and E_F are the energy of the conduction band, valence band, and the Fermi level, respectively, while \wedge_{air} is the thickness of the space-charge layer, and $eV_{surface}$ is the potential barrier. The conducting electrons are represented by e^- and the donor sites are also represented by +.	39
2.14	Schematic band structure and conduction process for a well-sintered ceramic and thin film gas sensor	41

LIST OF FIGURES (Continued)

Figure		Page
2.15	Schematic band structures for a less sintered ceramic, nanocrystallite or very thin film gas sensor with and without inflammable gas	43
2.16	Schematic intergranular contacts for CO sensing in an n-type oxide	44
2.17	The multiple reaction processes of TiO ₂ semiconductor under UV illumination: (1) electron excitation of semiconductor; (2) non-trapped exciton recombination; (3) deep trapping of (a) VB holes and (b) CB electrons; (4) shallow trapping of (a) holes and (b) electrons; (5) reductive foundation by shallowly trapped electrons; (6) oxidative foundation by shallowly trapped holes; (7) recombination of deeply trapped excitons and (8) recombination of shallowly trapped excitons	46
2.18	The several possible reactions with activated oxygen in the mechanism of photooxidative mineralization of organic compounds	51
3.1	Schematic diagram of an FSP reactor set-up	60
3.2	Spray flame appearances of (a) undoped ZnO and (b) 0.5 at% (c) 1 at% (d) 2 at% (e) 3 at% and (f) 5 at% Sn-doped ZnO	61
3.3	Schematic diagram of gas-sensing measurement	63
3.4	Schematic diagram of photocatalytic activity measurement	65

LIST OF FIGURES (Continued)

Figure		Page
4.1	XRD patterns of undoped ZnO and Sn-doped ZnO nanostructures synthesized by FSP with different Sn concentrations	66
4.2	Crystallite size in (100), (002) and (101) planes, from XRD, of undoped ZnO and Sn-doped ZnO nanostructures synthesized by FSP with different Sn concentrations	68
4.3	(a) The calculation of XRD lattice aspect ratio (L/D_a) using the (100) and (002) crystallite sizes of 0–5 at% Sn-doped ZnO, corresponding with (b) ZnO hexagonal-close-packed wurtzite structure	69
4.4	The trend of XRD-crystallite size, BET-equivalent average primary particle diameter and specific surface area of 0–5 at% Sn-doped ZnO synthesized by FSP	70
4.5	TEM images of (a) undoped ZnO, and (b) and (c) 5 at% Sn-doped ZnO nanostructures	72
4.6	SEM images of (a) undoped ZnO, (b) 2 at% Sn-doped ZnO and (c) 5 at% Sn-doped ZnO nanostructures with EDS analysis of all covered area of the SEM image, inserted at the side of the images	73

LIST OF FIGURES (Continued)

Figure		Page
4.7	FESEM-EDS analysis of 2 at% Sn-doped ZnO sensing film: (a) cross-section FESEM image, (b) EDS line scan mode indicated as the corresponding signal of the elements composition, (c) top view before gas sensing test and (d) top view after gas sensing test	75
4.8	Relationship between (a) 400 ppm $(\text{CH}_3)_2\text{CO}$, (b) 1,000 ppm $\text{C}_2\text{H}_5\text{OH}$, (c) 50,000 ppm H_2 , and (d) 50,000 ppm CH_4 response/response time, and operating temperatures	77
4.9	Change in the conductivity of undoped ZnO, and 2, 3 and 5 at% Sn-doped ZnO sensors under exposure to (a) $(\text{CH}_3)_2\text{CO}$, (b) $\text{C}_2\text{H}_5\text{OH}$, (c) H_2 , and (d) CH_4 at 400°C during backward cycle	81
4.10	The gas sensing response of 5 at% Sn-doped ZnO to $\text{C}_2\text{H}_5\text{OH}$ and H_2 , and 3 at% Sn-doped ZnO to $(\text{CH}_3)_2\text{CO}$ and CH_4 , as a function of concentration at operating temperature of 400°C	84
4.11	The gas response of undoped ZnO, and 2, 3 and 5 at% Sn-doped ZnO sensors at 100 ppm of $(\text{CH}_3)_2\text{CO}$ and $\text{C}_2\text{H}_5\text{OH}$, and at 10,000 ppm of H_2 and CH_4 under the operating temperature of 400°C	85

LIST OF FIGURES (Continued)

Figure		Page
4.12	SEM image comparisons in the same scale of (a) original FSP-made 2 at% Sn-doped ZnO nanostructures, and (b) prepared 2 at% Sn-doped ZnO film	87
4.13	UV-Vis absorption spectra of ZnO nanostructures with 0–5 at% Sn doping concentration	89
4.14	First derivative of absorbance (abs.) with respect to photon energy (E) of (a) undoped ZnO, (b) 0.5 at% Sn-doped ZnO, (c) 2 at%, (d) 3 at% Sn-doped ZnO, and (e) 5 at% Sn-doped ZnO	91
4.15	Photodegradation of C ₆ H ₅ OH with initial concentration (C ₀) of 10 mg C/l over undoped and Sn-doped ZnO nanostructures under UVA irradiation: (a) change in C ₆ H ₅ OH concentration as a function of irradiation time, and (b) pseudo first-order degradation rate constant of undoped ZnO	94
4.16	Change in CH ₃ OH concentration as a function of irradiation time on photodegradation of CH ₃ OH with initial concentration (C ₀) of 500 µg C over undoped and Sn-doped ZnO nanostructures under UVA irradiation	98
B.1	Photocatalytic calibration curve	135
B.2	Repeated testing on phenol photodegradation	136

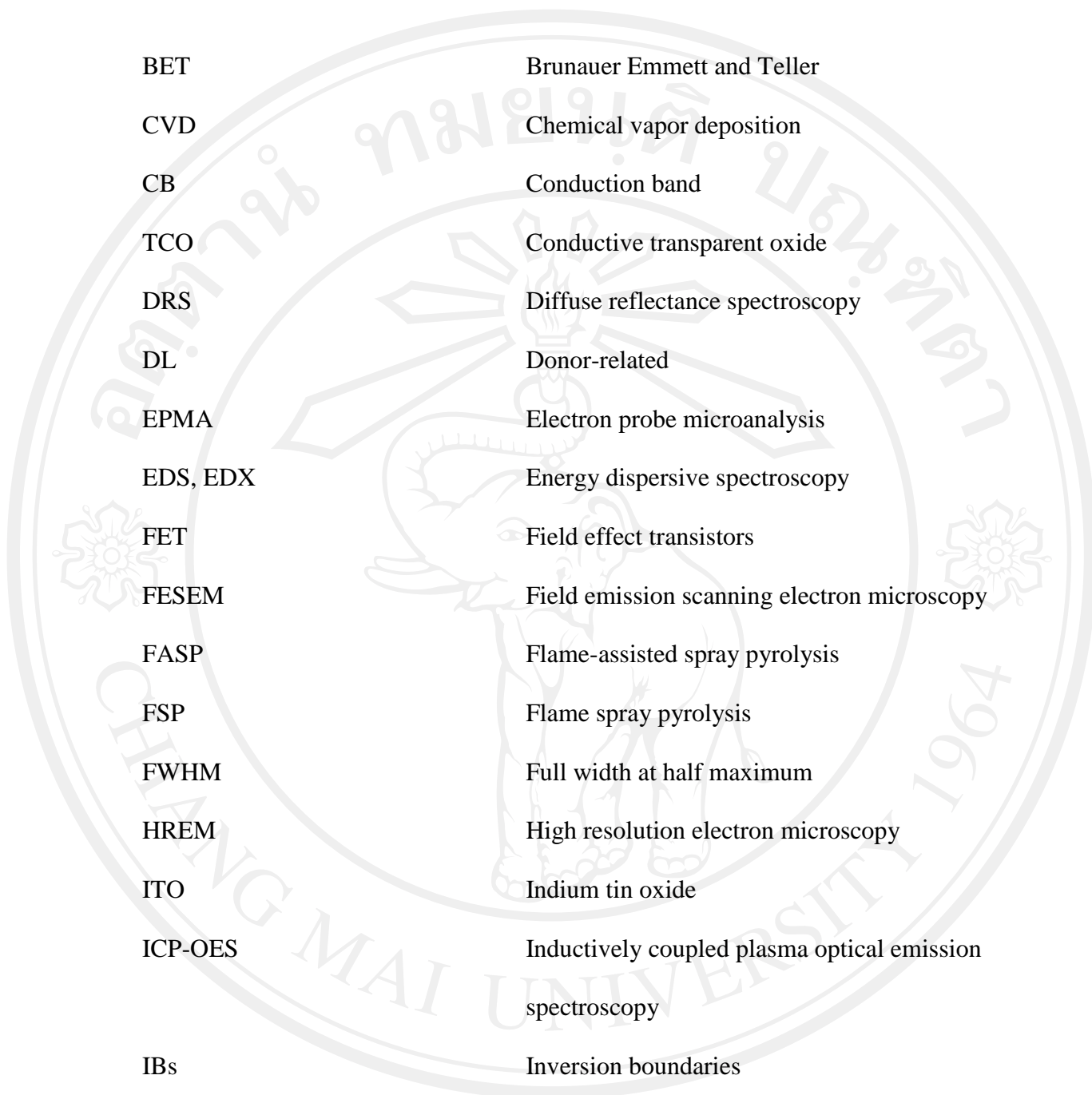
ABBREVIATIONS AND SYMBOLS

E_A	Activation energy
K	Adsorption equilibrium constant
\wedge	Band bending depth
E_g	Bandgap energy
T_{bp}	Boiling point
k_B	Boltzmann constant
H_{CHEM}	Chemical energy
β	Collision frequency
C	Concentration
C_t	Concentration as a function of temperature
E_C	Conduction band edge
R^2	Correlation coefficient value
d_{XRD}, d_{hkl}	Crystallite size from XRD
L_D	Debye length
$T_{d/mp}$	Decomposition/melting point
Γ	Density of sites covered by adsorbate
Γ^0	Density of surface adsorption sites
D_a	Diameter
D	Diffusion coefficient

E_D	Dissociation energy
r_c	Distance of chemical bond on surface
n_d	Donor concentration
n_{eff}	Effective density of states
e^-	Electron
χ	Electron affinity
e	Electron charge
m_e	Electron effective mass
Θ	Equilibrium coverage
E_F	Fermi level
θ	Fractional coverage
ν	Frequency of light
a_s	Fused sphere surface area
τ	Grain boundary diffusion
$D_b(T)$	Grain boundary diffusion coefficient as a function of temperature
w_b	Grain boundary width
h^+	Hole
m_h	Hole effective mass
I	Ionization potential
L	Length
A	Light absorption coefficient

E_U	Localized states
B	Magnetic flux densities
Ω	Molar volume of diffusing species
N_i	Net impurity concentration
N	Number concentration of particles
N_d	Number of dopant donor atoms
p_{gas}	Partial pressure of gas
θ	Peak position
β_k	Peak width at half maximum intensity
l	Penetration depth of light into solid
ϵ_0	Permittivity of free space
ϵ_s	Permittivity of semiconductor
H_{PHY}	Physical energy
h	Planck's constant
P	Pressure
d_{BET}	Primary particle size from BET
r	Radius
k	Rate constants
r	Reaction rate
G	Sensor conductance
R	Sensor resistance
k_s	Shape factor

c	Speed of light
G	Standard Gibbs energy
ϵ	Static dielectric constant
a	Surface area
θ_s	Surface coverage
V_s	Surface potential
eV_{surface}	Surface potential barrier
w	Surface space charge layer
E_s	Surface state energy level
N_s	Surface state density
γ	Surface tension
T	Temperature
W	Thickness of space-charge layer
τ_{tr}	Transit time of photogenerated charges
E_t	Trap energy
λ	Wavelength of light
ρ	Weighted density
AL	Acceptor-related
ARPES	Angle-resolved photoelectron spectroscopy
APs	Antiphase boundaries
AFM	Atomic force microscope
BP	Basal plane



BET	Brunauer Emmett and Teller
CVD	Chemical vapor deposition
CB	Conduction band
TCO	Conductive transparent oxide
DRS	Diffuse reflectance spectroscopy
DL	Donor-related
EPMA	Electron probe microanalysis
EDS, EDX	Energy dispersive spectroscopy
FET	Field effect transistors
FESEM	Field emission scanning electron microscopy
FASP	Flame-assisted spray pyrolysis
FSP	Flame spray pyrolysis
FWHM	Full width at half maximum
HREM	High resolution electron microscopy
ITO	Indium tin oxide
ICP-OES	Inductively coupled plasma optical emission spectroscopy
IBs	Inversion boundaries
JCPDS	Joint Committee on Powder Diffraction Standards
LD	Laser diodes
LED	Light emitting diodes
MO	Methyl orange
MB	Methylene Blue

ลิขสิทธิ์มหาวิทยาลัยเชียงใหม่
Copyright © by Chiang Mai University
All rights reserved

MBE	Molecular beam epitaxy
NBs	Nanobelts
NSs	Nanostructures
NBE	Near-band-edge
OECD	Organisation for Economic Co-operation and Development
PES	Photoelectron spectroscopy
PL	Photoluminescence
pgms	Platinum group metals
POQ _{hkl}	Preferred orientation
PLD	Pulse laser deposition
RPP	Rapid photothermal processing
RHEED	Reflection high-energy electron diffraction
RMS	Root mean square
SAED	Selected area electron diffraction
SZO	Sn-doped ZnO
SSA	Specific surface area
SILAR	Successive ionic layer adsorption and reaction
TEM	Transmission electron microscopy
TFT or TTFT	(Transparent) thin film transitions
TSCD	Two-stage chemical deposition
UAs	Unsaturated alcohols
USP	Ultrasonic spray pyrolysis
UV-vis	Ultraviolet-visible

VB	Valence band
VFS	Vapor-fed flame synthesis
VLS	Vapor-liquid-solid
XRD	X-ray diffraction
XPS	X-ray photoelectron spectroscopy

ลิขสิทธิ์มหาวิทยาลัยเชียงใหม่
Copyright© by Chiang Mai University
All rights reserved